Nitric Oxide PLIF Visualization of Simulated Fuel-Air Mixing in a Dual-Mode Scramjet

Luca M. L. Cantu[*], Emanuela C. A. Gallo[†], Andrew D. Cutler[‡],
The George Washington University, Mechanical and Aerospace Engineering, Washington, DC, 20052

Brett F. Bathel[§], Paul M. Danehy[**]
NASA Langley Research Center, Advanced Measurements and Data Systems Branch, Hampton, VA, 23681

Robert D. Rockwell[††], Christopher P. Goyne[‡‡], James C. McDaniel[§§]
University of Virginia, Mechanical and Aerospace Engineering, Charlottesville, VA, 22904

Nitric oxide (NO) planar induced laser fluorescence (PLIF) measurements have been performed in a small scale scramjet combustor at the University of Virginia Aerospace Research Laboratory at nominal simulated Mach 5 flight. A mixture of NO and N_2 was injected at the upstream end of the inlet isolator as a surrogate for ethylene fuel, and the mixing of this fuel simulant was studied with and without a shock train. The shock train was produced by an air throttle, which simulated the blockage effects of combustion downstream of the cavity flame holder. NO PLIF signal was imaged in a plane orthogonal to the freestream at the leading edge of the cavity. Instantaneous planar images were recorded and analyzed to identify the most uniform cases, which were achieved by varying the location of the fuel injection and shock train. This method was used to screen different possible fueling configurations to provide optimized test conditions for follow-on combustion measurements using ethylene fuel. A theoretical study of the selected NO rotational transitions was performed to obtain a LIF signal that is linear with NO mole fraction and approximately independent of pressure and temperature.

I. Introduction

Planar laser induced fluorescence (PLIF)[1] is an instantaneous, spatially-resolved optical measurement technique that involves molecular excitation for both quantitative measurements and flow visualization. A laser, first expanded into a planar sheet and then focused in the measurement region, is accurately tuned to a specific absorption transition of the target molecule; for a certain finite time (fluorescence life time), a spontaneous emission of radiation from an upper energy level (fluorescence) is emitted from the illuminated region at a longer wavelength. When the molecule emits energy at the same wavelength the process is called resonance fluorescence. Usually some energy can be lost due to molecular collisions, a process known as collisional quenching. Collisions may also cause rotational and vibrational energy transfers to other adjacent states, usually resulting in additional spontaneous fluorescence emission lines at longer wavelengths compared to the laser. A schematic representation of this process is shown in the energy diagram in Figure 1.

---

[*] Ph.D. Candidate. Member AIAA
[†] Ph.D. Candidate. Member AIAA
[‡] Professor. Associate Fellow AIAA
[§] Research Scientist. Senior Member AIAA
[**] Research Scientist. Associate Fellow AIAA
[††] Senior Scientist, Member AIAA
[‡‡] Associate Professor, Associate Fellow AIAA
[§§] Professor, Associate Fellow AIAA

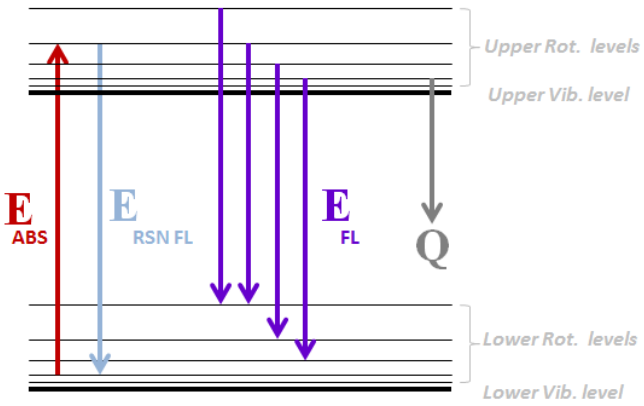

Figure 1: LIF energy diagram

Due to its capability to detect fluorescence of one flame radical or minor species at a time in part per million ranges, PLIF is a very suitable technique in hot, high-speed flow environments.[2,3,4,5] Several studies used the PLIF technique for visualization of the high-speed combustion and mixing processes: Hartfield at al.[6] and later Donohue et al.[7] performed a quantitative mixing study using iodine PLIF. Takahashi et al.[8] investigated mole fraction distribution and density using acetone as tracer. Rasmussen et al.[9] used OH and CH_2O-PLIF to study a cavity flame stabilization mechanism. Donbar et al.[10] used OH-PLIF in an ethylene and JP-7 combustion study. Gaston et al.[11] used PLIF to determine mixing performance parameters and performance of H_2 fuel injectors using PLIF. Gruber et al.[12] investigated a supersonic cavity design using NO and OH PLIF, injecting reacting and non-reacting ethylene. Barnes et al.[13] used acetone PLIF to determine fuel distribution in a directly injected cavity. Thakur et al.[14] determined concentration distribution behind a cavity step. Rossmann et al. used PLIF with NO as a tracer to investigate a mixing layer in low pressure hypersonic flow[15] and to image a compressible shear layer.[16]

Of particular interest is the mixing of fuel and air in a "dual-mode" scramjet combustor: in a high speed combustor, the flame produces a thermal blockage due to the heat release of combustion, hence a pressure rise that propagates into the isolator; a shock train is generated affecting the quality of the fuel-air mixing. In this paper, a mixing study of an ethylene fuel simulant was performed at the entrance plane of the cavity flame-holder. The goal of this study was to identify the most uniform premixed mixture of fuel and air so that flame propagation is controlled by combustion processes (i.e. by chemistry and the diffusion of reactant/product species and heat) rather than by fuel-air mixing processes, which would allow results to be compared to the large literature of premixed flame experiments. For this purpose an unheated mixture of nitrogen (N_2) and nitric oxide (NO) was chosen to simulate an ethylene fuel, due to the similar molecular weight, and injected at the inlet isolator upstream of the cavity. A frequency-doubled tunable laser was tuned at ~226 nm to excite specific absorption transition of NO; images of NO fluorescence were recorded at the entrance cavity plane where stronger fluorescence indicated higher fuel concentration. This allowed visualization of both the effects of various fuel injection configurations and the effect of the shock train, which enabled identification of best, most uniform premixed case. Different equivalence ratios, injector configurations, and tunnel operational conditions were tested in a continuous scramjet tunnel facility. The optimum mixing conditions are identified in the current paper and should dictate the test conditions for subsequent hydroxyl (OH) PLIF, particle image velocity (PIV), width enhanced coherent anti-Stokes Raman scattering (WIDECARS), and formaldehyde (CH_2O) PLIF measurements of ethylene-air combustion in the same facility.

II. Experimental Setup – Facility

All the experiments were performed at the University of Virginia Supersonic Combustion Facility (UVaSCF), a small scale, vertically oriented, electrically heated, continuous flow, optically accessible, direct-connect scramjet wind tunnel, described in details by Rockwell et al.[17] and Krauss et al.[18,19] The UVaSCF uses a Mach 2 nozzle to simulate a Mach 5 flight condition (with stagnation pressure p_0 = 300 kPa and temperature T_0 = 1200 K respectively) in the engine-shaped test section; the flow-path geometry is shown in Figure 2.

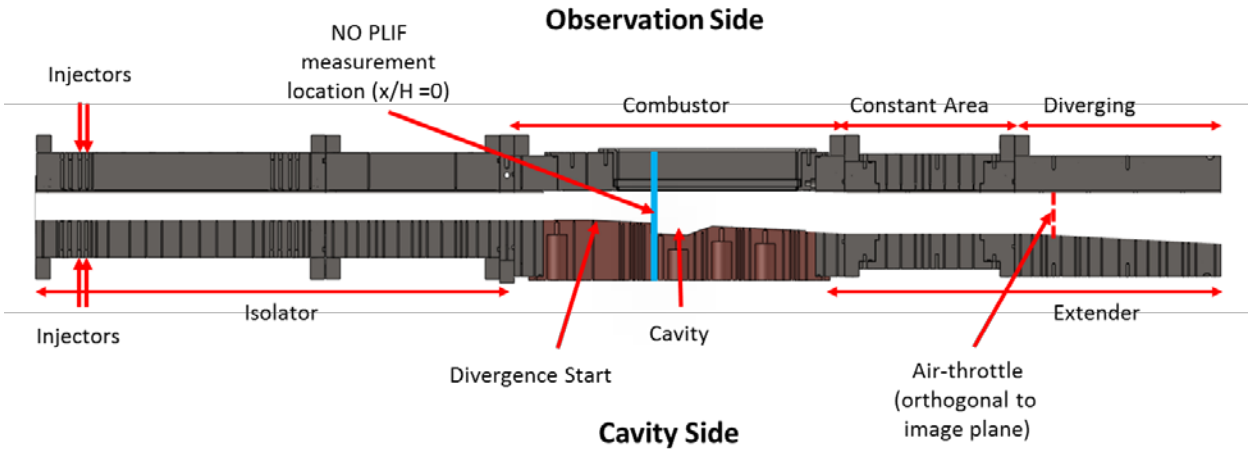

Figure 2. The scramjet duct geometry, injectors' location and test plane (blue line) for NO PLIF measurements

The model[20] consisted of inlet isolator, combustor, and extender sections. The constant-area-isolator section (44.5 H long, where H = 9.04 mm, height of the combustor cavity) was placed ahead of the combustor to contain the combustion induced shock train,[21] allowing the model to operate at higher equivalence ratio (ER = 15.29 $\chi_{fuel}/(1-\chi_{fuel})$). Two span-wise rows (spaced 6.35 mm apart) of three injectors per wall (1.27 cm apart, 1.25 mm diameter), perpendicular to and flush with the walls, were located at 55.33 H and 54.64 H from the start of the isolator.[22] In most of this experiment, a premixed 90% N_2 and 10% NO (mole fraction) fuel simulant was used in place of ethylene (C_2H_4) to study the mixing phenomenon without combustion. The similar molecular weight (the N_2-NO mixture weighs 28.21 g/mol, while C_2H_4 weighs 28.05 g/mol) meant that the mixing behavior of the fuel and simulant would be similar.

The combustor section diverged at an angle of 2.9°. A cavity (height H = 9.04 mm, length L = 5.25 H, and 22.5° closeout angle) was placed in the combustor, 64.5 H from the end of the isolator, to enhance the residence time of oxidizer and radicals for flame-holding purposes.[23] Two UV grade fused silica windows were mounted in the parallel side walls to provide optical access for the cross-plane laser sheet (described in Section III) for flow visualization. All measurements were taken at a measurement plane just upstream of the cavity step, which is defined as x/H = 0. The extender was divided into two sections: a constant area section, 16.47 H long, and a diverging section, 18.92 H long, angled by 2.9° on the cavity side wall. At x/H = 37, inside the extender section, pressurized air was injected into the flow from a pair of slots, located in both parallel side walls, providing a backpressure effect: this was done to simulate the pressure rise during combustion while operating with a non-reacting flow. By controlling the air pressure through a throttle, it was possible to move the shock train inside the isolator; this shock train promoted a high degree of mixing of fuel and air in the isolator by increasing the level of turbulence and thickening the boundary layer.

III. Experimental Setup – Laser and Optics

The laser and the optical system used in this experiment are mounted on a mobile cart, primarily used to perform coherent anti-Stokes Raman scattering (CARS) and width increased dual-pump enhanced (WIDE)CARS measurements, as described by Cutler et al.[24] and Gallo et al.[25] respectively. With respect to the previously described systems, OH PLIF and later NO PLIF were included to the capability of the laser cart: in this new configuration, it was possible to switch from one laser frequency and measurement technique to another with minor adjustments and to perform different types of measurements with a common mobile system.

Light from a 1064 nm, 20 Hz pulsed, Nd:YAG laser was frequency doubled to produce a 532 nm laser beam; this beam was used to pump a narrowband dye laser (Spectra Physics PDL-2) which excited a mixture of Rhodamine 590 and Rhodamine 610 laser dyes, optimized to obtain 570 nm light. The output of the dye laser was frequency doubled then mixed with the residual 1064 nm beam using two Spectra Physics Wavelength Extender (WEX) crystal modules which were removed from the WEX cabinet and placed on the mobile cart to produce ultra violet (UV) light at 226 nm. This light was used to excite ${}^{P}P_{11}(27)$, ${}^{Q}Q_{22}(24)$ and ${}^{S}R_{21}(8)$ NO lines (a more detailed

explanation is provided in Section IV). These transitions were selected because they minimize the pressure and temperature dependencies of the PLIF signal, as described by Fox et al.,[26] thereby making the fluorescence intensity sensitive only to the mole fraction of NO. The UV light exiting the WEX module was sent first to a periscope containing dichroic mirrors, in order to separate the 226 nm light from the other colors of light and to change the polarization to be horizontal. Then the light passed through a horizontally-oriented Pellin-Broca prism to further separate the 226 nm beam from all the other residual wavelengths which were sent to a beam dump. About 1% of the UV beam was sampled using a p-polarized reflection off an uncoated, quartz beam-splitter before exiting the laser cart: this reflection was split into two paths: the first one was sent to a photodiode connected to an oscilloscope to monitor the laser energy on a pulse to pulse basis; the second beam was directed to a lens-coupled fiber optic which was connected to a High Finesse WS-6L UV Wavemeter to continuously monitor the wavelength. It was important to continuously monitor the laser energy and wavelength since the PDL and the WEX crystals were sensitive to temperature variations and needed to be optimized before each run. Figure 3 shows the optical setup close to the measurement location.

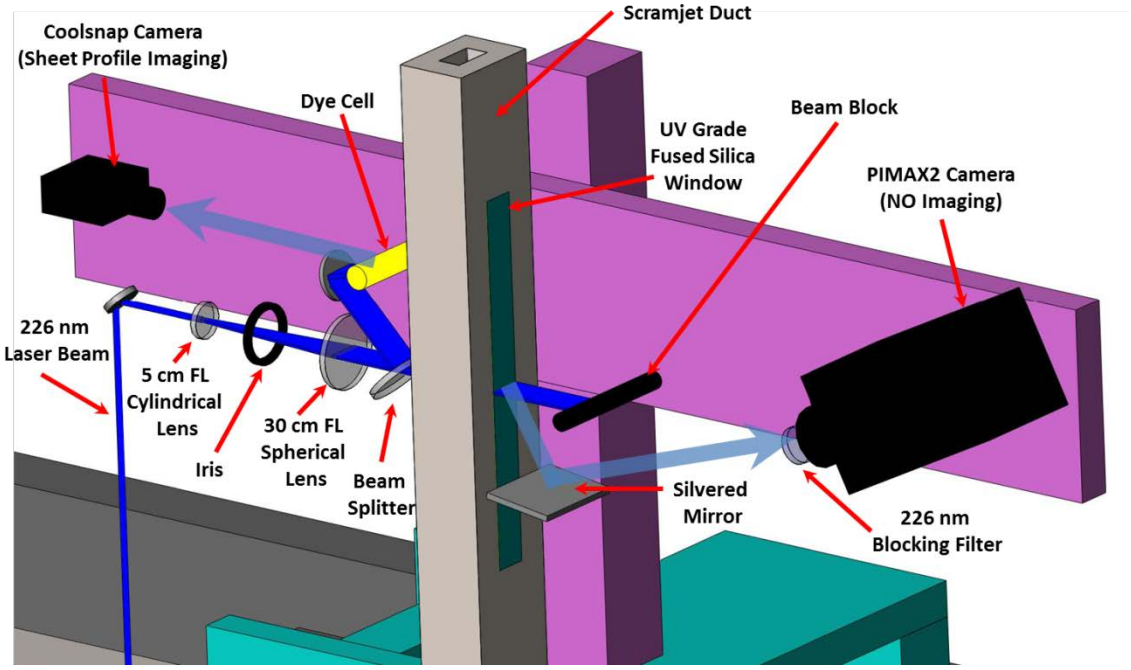

Figure 3. Optical setup in the test room

After exiting the cart, a UV mirror and a periscope sent the UV laser beam to a motorized vertical stage; the 226 nm light was first expanded into a sheet by a 5 cm focal length (FL) cylindrical lens then collimated in one direction by a 30 cm FL spherical lens which focused the other dimension of the laser beam to a thin waist roughly 100 microns thick. A 50 mm diameter, p-reflection, uncoated fused silica beam-splitter was placed in the beam prior to the beam entering the tunnel and the small portion (~1%) of the beam was reflected and used to illuminate a dye cell filled with a Rhodamine 590 solution. A Photometric Coolsnap:cf camera imaged fluorescence from the dye cell to record images of laser sheet's spatial profile which were used during data processing to correct for laser energy fluctuations. The laser sheet, which was oriented perpendicular to the free-stream, was directed through two UV grade fused silica windows, mounted on sides of the tunnel and containing the flow. The beam impacted on a beam block on the other side of the duct. An Intensified Coupled Charged Device (ICCD) PIMAX2 camera was used to record the PLIF signal on 512x512 pixel array. Since it was not possible to have a direct perpendicular camera view of the laser sheet, the PIMAX2 was angled ~39° with respect to the laser sheet, viewing an image reflecting off a square silvered mirror placed as close as possible to the tunnel. A Scheimpflug mount was also used to better focus the image since the camera view was not perpendicular to the image plane. Geometrical distortions, resulting from this imaging configuration, were corrected during the data analysis procedure described in Section V. A 226 nm blocking filter (Layertec GmbH, Germany, <1% transmission at 226 nm and >80% transmission at 235-280 nm) was placed in front of the lens of the PIMAX2 in order to eliminate scattered laser light. Resonant fluorescence was also blocked by this filter, helping minimize the effect of so-called radiative trapping (wherein emitted photons are

reabsorbed by the gas) on the recorded PLIF signal[27]. The PIMAX2 camera triggered the Coolsnap camera such that the images could be synchronized and a laser sheet correction could be applied for each single image acquired.

IV. Experimental Method – Choice of Laser Frequency

For this experiment, a new study was conducted for the selection of the optimal laser wavelength for the conditions expected in the combustor flow. A Matlab code written by Bathel was used to verify whether Fox et al.'s[26] selection of transitions provided temperature and pressure independence over the expected operational range of the combustor (T = 667-1100 K and p = 80-160 kPa). The code computed NO line positions using equations from Engleman et al.[28] and Palma[29] and coefficients from Danielak et al.;[30] collisional broadening and shift constants were computed based on work by DiRosa[31] and Vyrodov et al.,[32] while quenching constants were computed using values, coefficients, and relations from Settersten et al.[33] and Paul et al.[34]

Three spectrally-coincident NO rotational transitions, $^{P}P_{11}(27)$, $^{Q}Q_{22}(24)$ and $^{S}R_{21}(8)$, were selected in order to generate a LIF signal proportional to the mole fraction of NO and independent of temperature and pressure, as shown in prior work[26] and updated with calculations presented herein. Using the notation of Fox et al., a linear relationship between the fluorescence intensity and NO mole fraction occurs when $S_{LIF}=K\chi_{NO}$, where S_{LIF} is the fluorescence signal, χ_{NO} is the NO mole fraction and the variable K should ideally constant for different temperatures and pressures likely to occur in the experiment. Figure 4 shows the value of K for various spectral lines of NO, normalized by the maximum K in the range of the calculations, plotted as a function of temperature. Following Fox et al., implicit in the variation of temperature shown here is a variation in mole fraction NO typical of what would be expected in this present study of fuel-air mixing. Mole fraction fuel simulant (10% NO, 90% N_2) is assumed to be one at 250 K (typical conditions of the fuel at the exit of the injector), zero at 1100 K (typical conditions in the free stream in the presence of inlet shock train); intermediate conditions were computed assuming adiabatic mixing of these two gases. This figure shows that the $^{S}R_{21}(8)$ transition has high signal at low temperatures (and low signal at high temperatures), while $^{P}P_{11}(27)$ and $^{Q}Q_{22}(24)$ transitions have the opposite behavior. The top (bold black) line represents the sum of the contributions from these three lines, resulting in a quasi-constant value of K close to one, and a linear dependence of S_{LIF} on χ_{NO}, the mole fraction of NO.

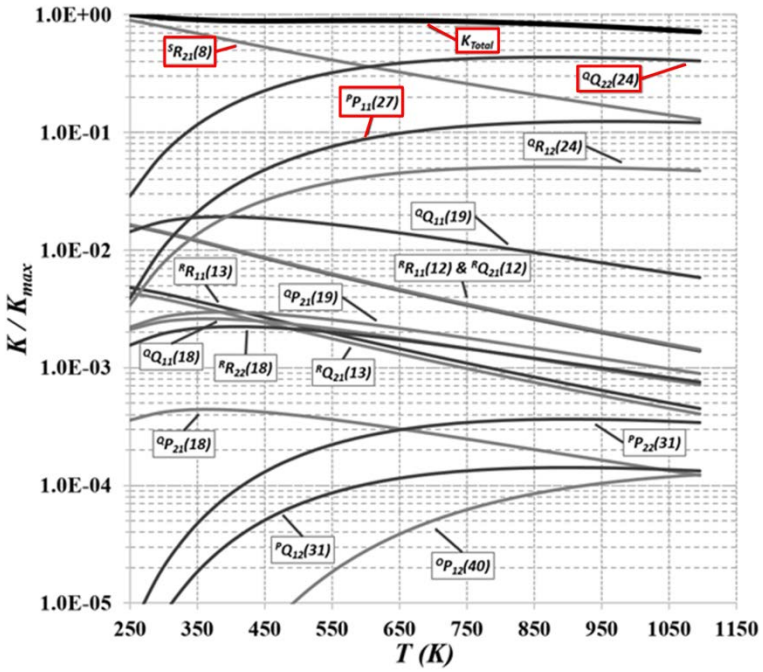

Figure 4. LIF signal temperature dependence of different spectral excitation lines. Calculations performed at 120kPa with fuel mixture of 10% NO – 90% N_2. The bold line respresents the sum of the contributions from three spectrally-coincident lines excited in this experiment: $^{P}P_{11}(27)$, $^{Q}Q_{22}(24)$ and $^{S}R_{21}(8)$

Figure 5 shows the simulated LIF signal as a function of both fuel-simulant mole fraction and static temperature. By selecting a frequency (44283.13 cm^{-1}), slightly different from that originally used in the work of Fox et al.[26] (44282.38 cm^{-1}), a LIF signal that varies nearly linearly with fuel-simulant fraction is obtained with minimal dependence on static pressure. This LIF signal is particularly linear in the range of these measurements ($\chi_{fuel} < 0.065$, corresponding to ER = 1), indicated by the blue box on Fig. 5a). (Note that the larger range of fuel mole fractions is retained in this plot since it may find applications in other work where the fuel equivalence rations are larger.) Figure 5b shows the laser's spectral profile and how it overlaps with three important NO spectral absorption profiles plotted at different pressures and temperatures: the 1 cm^{-1} laser linewidth is wide enough to overlap all the selected lines without significant overlap with nearby lines located over 2 cm^{-1} away from the center frequency of the laser.

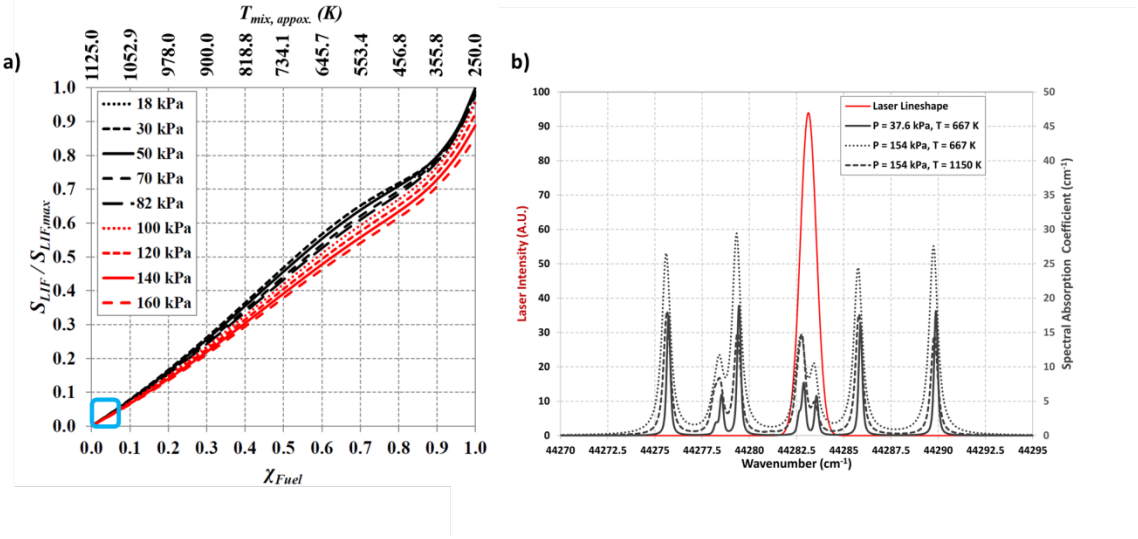

Figure 5. a) LIF signal is proportional to fuel mole fraction and fairly pressure-independent: blue box represents the region of interest explored during the tests; b) laser profile overlapped to NO rotational transitions at different pressures and temperatures

During the experiment, the WEX's crystal efficiency changed with room temperature, resulting in small variations in the frequency output of the laser. To prevent any significant shifts from the theoretical wavelength setting during the experiment, the laser's wavelength was monitored by a High Finesse Wavemeter (0.02 cm^{-1} accuracy) during the test. The wavelength of the laser was reset before each run to within 0.1 cm^{-1} of the chosen frequency. Consequently, a detuning study with respect to optimum laser wavelength (44283.13 cm^{-1}) was performed to investigate how changes in laser frequency might affect signal linearity. As shown in Figure 6, the large laser linewidth chosen (1 cm^{-1}) is relatively insensitive to detuning. By comparison, computations (not shown) performed with a narrower linewidth achievable with this same laser, showed a much higher sensitivity to changes in the laser frequency. Also, the figure shows that the LIF signal was less sensitive to line position when detuned to higher wavenumber rather than to lower wavenumbers. Figure 6 shows that the simulated LIF signal is linear at the anticipated conditions of the experiment (blue box), even as the laser frequency drifts from its nominal setting. The actual relationship between fuel fraction and fluorescence signal during the experiment is bounded by the three solid curves in the figure.

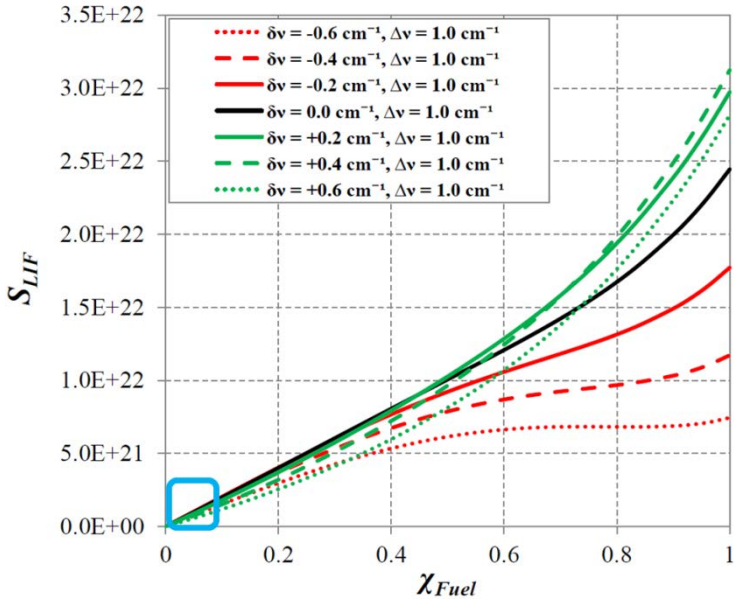

Figure 6. LIF signal versus fuel mole fraction for different laser detuning. Blue box shows range of current experiments, over which the LIF signal is fairly linear and insensitive to detuning

V. Experimental Method – Data Analysis

A statistically significant number of images (300 single shots for June 2014 tests, 500 single shots for August 2014 tests) were collected at 10 Hz for several injector configurations and equivalence ratios. All the recorded images were first background subtracted[35] then processed to correct for geometrical distortion[36] and laser intensity non-uniformities.

A background image, consisting of 100 single shots taken with the tunnel operating at test conditions but fuel off, was recorded after each run. This sequence of images were averaged and subtracted from the PI-MAX2 images to eliminate the effects of room light and scattered laser light from the tunnel wall that may affect the LIF signal.

To correct for image distortion, an image of a dotcard (a white card filled with equally spaced black squares) was recorded before each test at the laser plane location (x/H = 0), as shown in Fig.7a. The so-called *dotcard image* was first processed by subtracting a background image, and applying a threshold function to force each pixel to be either black or white, as shown in Figure 7b. The image was then compared with its original undistorted pattern (Fig. 7c) image and unwarped through the freeware ImageJ[37] software program, using the UnwarpJ[38] plug-in, resulting in the unwarped image in Fig. 7d. The unwarping parameters were saved and applied to all the experimentally recorded images to remove perspective and other distortions.

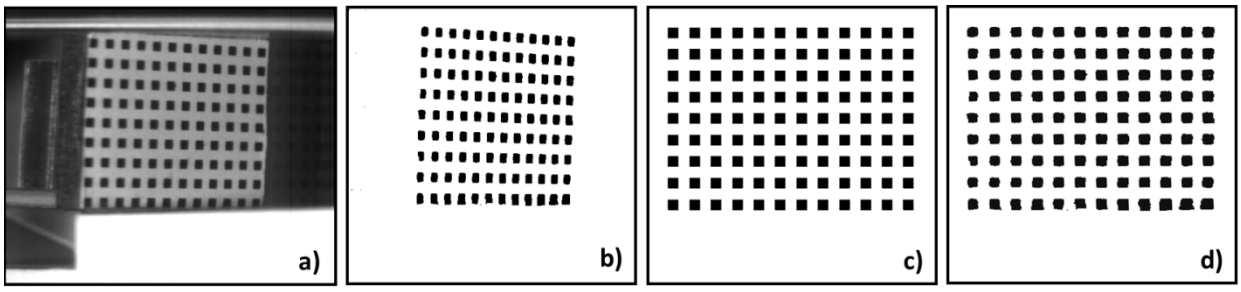

Figure 7. Dotcard dewarping procedure: a) raw dotcard image acquired with the dotcard placed in the plane of the laser sheet; b) processed dotcard with background removed and threshold applied; c) original dotcard; d) dewarped dotcard after application of UnwarpJ transformation.

Each single-shot PI-MAX2 image was divided by a reference image derived from the simultaneously-acquired Coolsnap image to correct for the effect of laser sheet non-uniformities. The procedure for generating the reference

image was developed as follows. A “fringed” card was placed in the path of the laser sheet to break the light sheet into several non-evenly spaced stripes. The resulting pattern in the light sheet was recorded by both the Coolsnap (Fig. 8a) and PI-MAX2 (Fig. 8b) cameras and the acquired images were averaged. A vertical line of pixels passing through the laser stripes was extracted from the Coolsnap image (Fig. 8a) to obtain the laser intensity profile. The same procedure was applied to the left side of the dewarped PI-MAX2 image (Fig. 8b), and the Coolsnap profile was stretched to match the PI-MAX2 profile (Fig. 8c). The Coolsnap profile was then expanded in the perpendicular direction and rotated. This image was overlapped with the original PI-MAX2 image (Fig. 8d) to verify the laser stripes from the PI-MAX2 image and processed Coolsnap image overlapped. The same process of extracting a vertical line of pixels, stretching, expanding in the perpendicular direction, and rotating was the applied to all Coolsnap images to generate the reference images. The reference images derived in this manner were smoothed using a Gaussian blur filter to remove the effects of single shot noise in the original Coolsnap image.

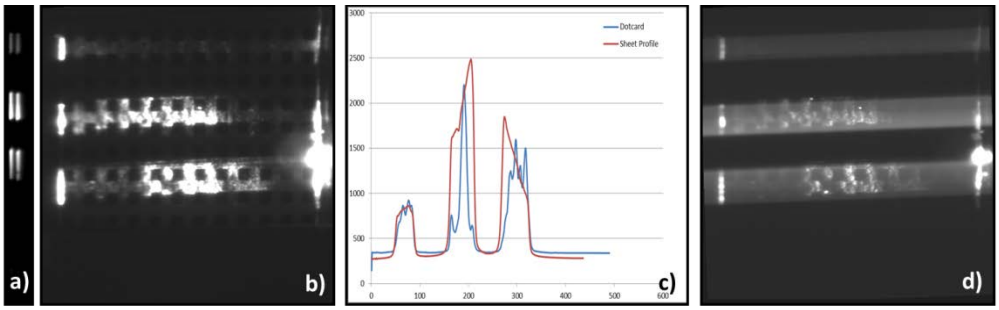

Figure 8. Laser sheet profile alignment to PLIF images: a) raw fringed laser sheet profile; b) unwarped masked dotcard; c) Coolsnap (sheet profile) and PI-MAX2 (imaging plane) plot profiles overlapped after applying stretching and rotation parameters; d) overlapping check by expanding the modified laser sheet profile (light white lines) to the dotcard image size

All the PLIF images were processed to correct for distortion and laser intensity non-uniformities as described above. An example of the result is shown in Fig. 9a. The images were then rotated 180° to match the coordinate system of previous work, cropped, and false colors added for a better visualization (Fig. 9b). An average was calculated from each stack of images from a given run condition, as shown in Fig. 9c.

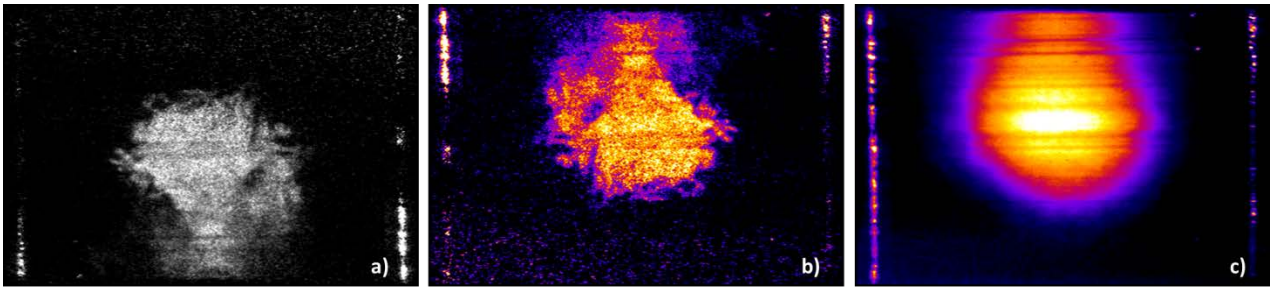

Figure 9. Final result of image processing of single injector on cavity side centerline (ER=0.09, shock train off): a) PLIF single-shot image corrected for distortion and laser intensity non-uniformities; b) PLIF image rotated 180° and false color added; c) averaged over the full set of 300 images.

Some horizontal lines are visible on the images in Fig. 9, most noticeably in Fig. 9c. This effect was due to accumulation of deposits on or chips in the facility windows which attenuated the laser sheet as it passed through the windows. An unheated run performed under humid conditions, prior to the high-temperature runs, may have been responsible for faster deterioration of the windows for the runs obtained this day. The windows visually appeared dirty after the runs were completed.

VI. Results

The fuel injectors were designed to operate independently. This flexibility allowed injecting from one side only, or from both sides, with symmetrical or non-symmetrical flow rates. By varying the injection pressure of the premixed fuel surrogate, it was possible to change the ER in the range of 0.00-0.45. Though it was possible for the fuel system to provide higher fuel flow rates, higher ERs were not tested since, in combustion cases, the shock train would propagate upstream of the injection sites (which caused the flame to jump forward and attach to the injectors). As stated previously, the objective was to demonstrate cases where mixing was fully uniform at the plane at the leading edge of the cavity. For each ER case tested, the fuel was mixed with different degrees of uniformity by independently changing the pressure at the cavity- and observation-side injectors (*cav* denotes cavity side, while *obs* denotes observation side). The model was back-pressurized using the air-throttle mechanism to simulate (in a non-reacting flow) the pressure rise that would be seen in a combustion case; adjusting the back-pressure caused the leading edge of the shock train to occur at several different locations: x/H = -15, -30, -45 or no back-pressure applied (off, i.e. no shock train).

Different ERs, coupled with different injector split ratios and shock train locations were tested to identify the optimum mixture uniformity. All the cases were tested on two different days (June 13th and August 29th, 2014) and their relative configurations are reported in Table 1.

Date	Run	NO conc.	E.R.	Injector split cav/obs	Shock train [x/H]	Mixing Goodness
Jun 13th	3	10%	0.42	0.23/0.15	-45	81%
Jun 13th	3b	10%	0.42	0.23/0.15	-45	75%
Jun 13th	4	10%	0.31	0.31/0.00	-15	30%
Jun 13th	5	10%	0.31	0.155/0.155	-15	80%
Jun 13th	7	10%	0.31	0.155/0.156	off	69%
Aug 29th	4	10%	0.44	0.22/0.22	-45	86%
Aug 29th	5	10%	0.36	0.19/0.17	-45	87%
Aug 29th	6	10%	0.35	0.18/0.17	-30	88%
Aug 29th	7	5%	0.44	0.22/0.22	-45	90%
Aug 29th	8a	10%	0.22	0.22/0.00	-45	81%
Aug 29th	8c	10%	0.22	0.22/0.00	off	24%

Table 1. Summary of all tested cases, tested conditions and mixing goodness

The fluorescence signal intensity is proportional to the fuel mole fraction and independent of temperature and pressure, as described previously. The goal of the tests was to identify and provide the most uniformly premixed flow. Ideally, the fluorescence intensity would be completely uniform indicating perfectly mixed fuel air mixture at the equivalence ratio determined by the flow-rates and listed in the table. In reality, even in the best case, the flow showed some non-uniformities either due to unmixed fuel or artifacts of the experiment. In order to quantify this lack of uniformity to enable quantitative comparison between the different cases tested, a new parameter, *mixing goodness*, was introduced and defined as follows:

$$Mixing\ goodness = \left(1 - \frac{Standard\ Deviation}{Mean}\right) \times 100$$

This parameter was obtained by first averaging the full stack of images and then calculating the mean and standard deviation of the pixel values from this averaged image (not the standard deviation of the single-shot images). A higher mixing goodness denotes a more uniform image, indicating better mixing. Run numbers 6 and 7 (both recorded on August 29th) were found to be the optimal mixed cases with a mixing goodness of 88% (ER=0.35) and 90% (ER=0.44) respectively, which provide two different ER cases for further testing. Note that cases with ER less than about 0.3, the reliability of the operation of the flame holder is markedly reduced, so these cases have been established as the high and low ER limits of the current configuration.

Figures 10a-c show images from Run 4 acquired on June 13th, at ER of 0.31 and shock train located at x/H=-15. The images are oriented such that the cavity-side wall is at the top. A few single-shot images have been selected to

visually convey the variation in the instantaneous turbulent diffusion of the simulated fuel into the core flow. Figure 10d shows the averaged fuel simulant distribution.

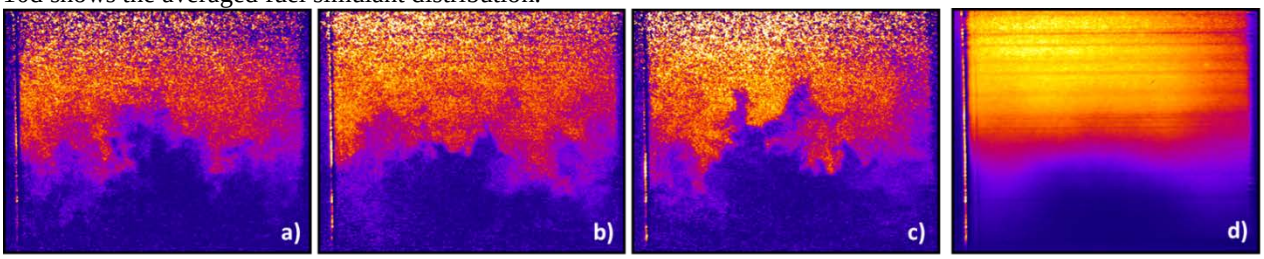

Figure 10. One-sided injection with shock train. Run 4 (June 13th) with ER=0.31 (injectors from only cavity side) and shock train at x/H=-15; a), b) and c) selected single shots; d) average

It can be inferred that a uniform mixed region was established close to the cavity-side wall, filling only half of the duct height. Hence, this case does not represent the desired fully premixed condition. Some shot noise is present in all the images, particularly close to the upper wall. This effect was due to a low NO fluorescence signal detected close to the upper wall, primarily due to a non-uniform laser sheet and in sufficient laser energy being available. However, this phenomenon is not detectable in the averaged image (Fig. 10d): the high number of images averaged together reduced this random error. For this test case, the streaks due to window contamination are more visible in the average image. These stripes may increase the value of the standard deviation, hence negatively affecting the calculated mixing goodness. While local mixing goodness in some parts of the flow is as good as 78%, the value calculated over the entire duct section was only 30%.

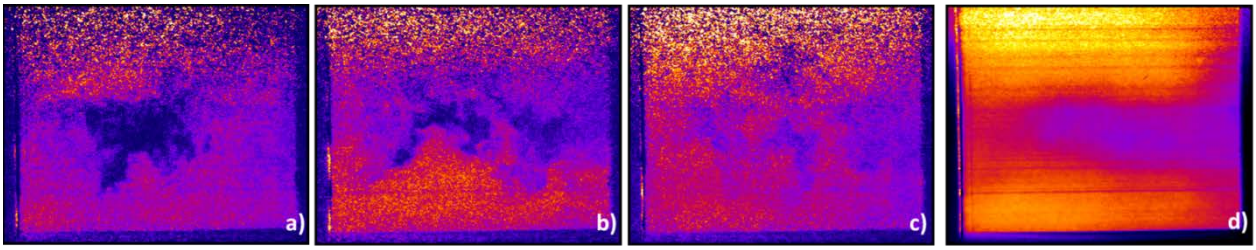

Figure 11. Two-sided injection without shock train. Run 7 (June 13th) with ER=0.31 (injection split equally) with no shock train (scramjet mode); a), b) and c) selected single shots; d) average

In contrast to the previous case, Fig. 11 (Run 7, June 13th) has the same total flow-rate of NO injected as in Fig. 10 but equally distributing the fuel simulant on both sides rather than one side. To achieve this overall ER = 0.31 setting, the mixture was equally injected at ER 0.155 on each side to see if more homogeneous mixing could be achieved. For this run, no back pressure was provided. Figures 11a-c are selected representative single shots taken from the same run: all of them indicate an unsteady unmixed region in the middle, a feature also seen in the average image (Fig. 11d). Despite the presence of the streaks, this run presents a mixing goodness of 69%, which is significantly better than the case with cavity-side only injection (Run 4, June 13th). The apparent hole (lack of signal) in the middle of the images indicates insufficient mixing to allow a fully premixed inflow plane. This suggests that applying backpressure is necessary to move the shock train upstream, closer to the injector, to promote better mixing.

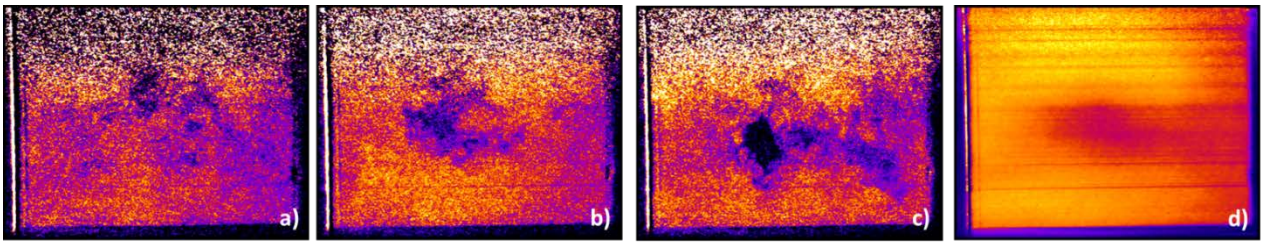

Figure 12. Two-sided injection with shock train. Run 5 (June 13th) with ER=0.31 (injectors split equally) and shock train at x/H=-15; a), b) and c) selected single shots; d) average

Figure 12 (Run 5, June 13th) shows the same conditions as Fig. 11 but with a shock train leading edge at x/H=-15. It can be seen that the addition of the shock train promoted mixing: the unmixed region in the middle is reduced, resulting in a more uniform image. Despite a low ER and a shock train close to the cavity, this run represents a mixing goodness of 80%. However, the remaining unmixed region at the center suggests that moving the shock train leading edge further upstream could provide a more uniform distribution of the fuel.

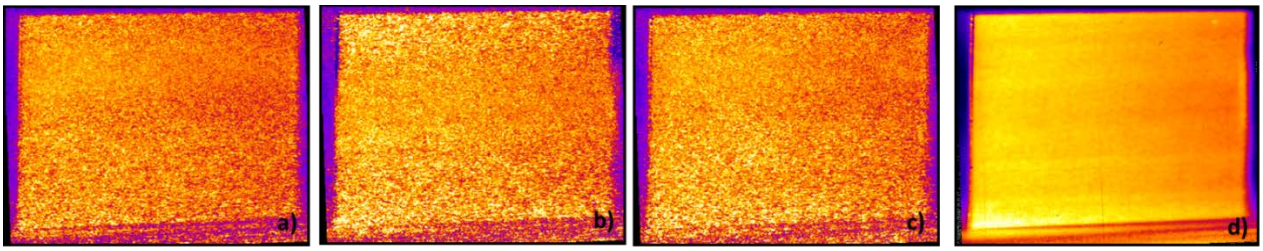

Figure 13. Two-sided injection with shock train further upstream. Run 7 (August 29th) with ER=0.44 (injection split equally on both sides of the duct) and the shock train at x/H=-45; a), b) and c) selected single shots; d) average

Figure 13 (Run 7, August 29th) is a richer mixture compared to Fig. 12. Also, a higher back pressure was applied with the air throttle to increase the turbulent mixing with the expectation of reaching a better mixture uniformity. At an ER of 0.44 (0.22 ER injection at each side) with a shock train located at x/H=-45, the most homogeneous mixing was obtained. For this set of experiments, the windows were replaced with freshly polished and cleaned windows and the averaged image (Fig. 13d) does not show any undesired streaks due to window defects. The noise is more uniformly distributed throughout the plane of interest, since a better laser energy distribution profile was obtained and later corrected in the image processing. The resulting single-shot fluorescence (Fig. 13 a, b, and c) is well-distributed vertically in the images, though a noticeable difference is observed from left to right. This is presumably caused by attenuation of the laser sheet due to absorption of the laser light by the NO molecules: since the laser sheet was sent from left to right, less laser energy was available to excite the molecules on the right. A mixing goodness of 90% was found, indicating this condition (Run 7, August 29th) to be the best case for the upper ER limit. For the lower ER limit, Run 6 (August 29th) was found to be the best case: an ER of 0.35 with injection split equally on both sides and a shock train at x/H=-30 resulted in uniform mixing with a mixing goodness of 88% (images not shown in this paper).

In order to determine if the left-to-right reduction in fluorescence intensity was indeed due to absorption of the laser sheet by NO or it was caused by true spatial non-uniformity of NO mole fraction, a case with a reduced NO concentration fuel simulant was tested. The results for two similar cases are compared in Figure 14.

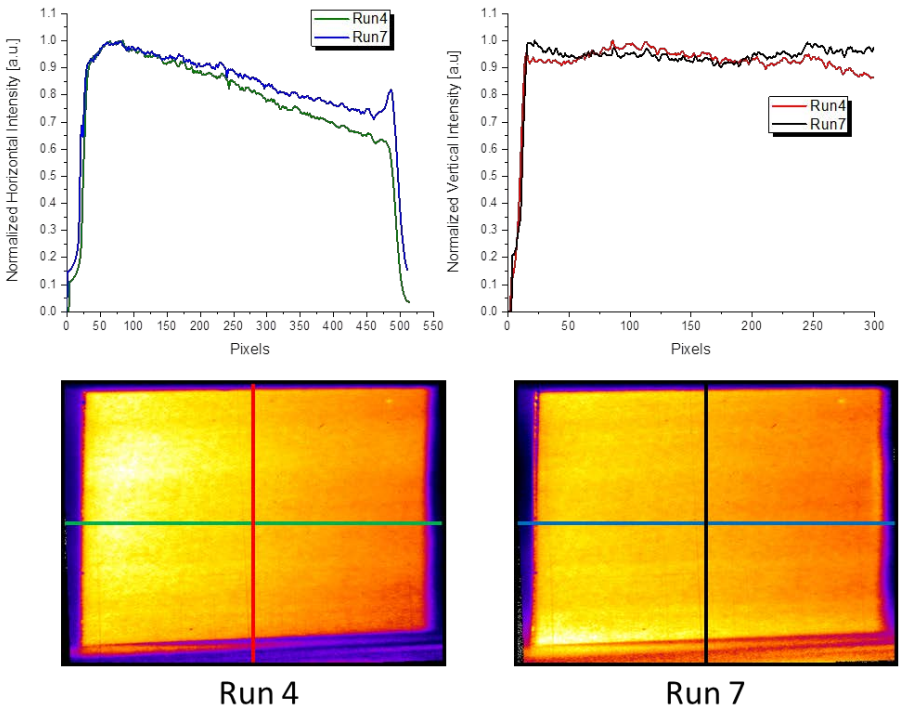

Figure 14. Normalized fluorescence intensity comparison between Run 4 and Run 7 (August 29th): both runs were with ER=0.44 (injector flows split equally) and shock train at x/H=-45. Run 4 had a mixture of 90% N_2 - 10% NO, while Run 7 was 95% N_2 - 5% NO. The plot on the top left shows a horizontal line profile taken in the middle of both images (lines green and blue); the plot on the top right shows a vertical line profile taken at the middle of both images (lines red and black).

Figure 14 shows averaged images for Run 4 and Run 7 (August 29th). With respect to Run 4, the NO concentration was halved in Run 7, maintaining the same injected flow rate by simply increasing the amount of N_2. Experimentally, the laser sheet was sent from left to right and, as predicted, the effect of absorption is more pronounced when more NO is injected (Run 4, 90%N_2-10%NO). The graph on the top right represents the normalized intensity profile taken on a line drawn vertically through the centerline of both images. The difference between the runs is small; the vertical laser sheet variation is ±5% (with respect to Run 7) and it can be considered constant along this direction. In addition, this variation can be considered an estimate of the errors in correcting for laser sheet non-uniformities (described above in Section V). The graph on the top left represents the normalized intensity profile taken on a line drawn horizontally through centerline of both images: the green line (Run 4) drops faster than the blue one (Run 7) supporting the hypothesis that the absorption of the laser intensity by NO is the cause of the declining intensity. In fact, Run 7 is slightly more uniform than Run 4 (90% vs. 88%); however the lower NO concentration yielded poorer quality single shot images in Run 7 compared to Run 4.

VII. Conclusions

An NO-PLIF optical system was integrated onto an existing laser cart so that three laser techniques (NO-PLIF, OH-PLF, and the Raman-based CARS technique) can be employed using the same mobile system.

Three spectrally coincident NO rotational excitation transitions, $^{P}P_{11}(27)$, $^{Q}Q_{22}(24)$ and $^{S}R_{21}(8)$, were chosen to provide a fluorescence signal proportional to mole fraction while being largely insensitive to variations in pressure and temperature. Theoretical calculations based on previous work were successfully extended to the range of conditions relative the present work-up to 1200 K and 160 kPa to simulate the test conditions in the engine of a scramjet flying at nominal Mach 5. LIF signal was found to be linear with the NO mole fraction in the region of the tested equivalent ratios. An optimum laser wavelength (44283.13 cm^{-1}) and laser linewidth (1 cm^{-1}) were selected to

excite these transitions at the expected test temperatures and pressures. A laser-detuning study was also performed and the signal was found to remain linear with NO mole fraction, independent of laser frequency variation, in the region of interest explored during the tests.

NO PLIF images were successfully acquired in a scramjet combustor at the cavity entrance plane, running with an unheated ethylene fuel surrogate (10% NO / 90% N_2) injected into an electrically-heated air stream. Images were processed to remove background (i.e. room light, laser scattered light, etc.) and to correct for geometrical perspective and camera lens distortions and for laser non-uniformities. Different ERs were tested to simulate combustion cases. An air-throttle mechanism was used to simulate the effect of combustion-induced pressure rise when employing a non-reacting fuel simulant. Variation of injection configuration (via different injector split ratios) and shock train locations were performed to identify the best mixing cases. Results were analyzed and compared using a newly defined mixing goodness parameter. A couple of cases at two different ERs satisfied the objective of the test and were identified as the most uniform cases: Run 7 (August 29th) with ER=0.44 (injection split equally on both sides of the duct) and the shock train at x/H=-45 showed mixing goodness of 90%; Run 6 (August 29th) with ER=0.35 (injection split equally on both sides of the duct) and the shock train at x/H=-30 showed mixing goodness of 88%. Both cases will be used as test conditions for subsequent ethylene-air combustion tests in the same facility.

VIII. Acknowledgments

This research was funded by the National Center for Hypersonic Combined Cycle Propulsion (NCHCCP), grant No. FA-9550-09-1-0611, with Dr's. Chiping Li (AFOSR), Aaron Auslender (NASA), and Rick Gaffney (NASA) serving as technical monitors. The authors are also thankful to Justin Kirk (University of Virginia) and Damien Lieber (University of Virginia) for their precious help in operating and monitoring the facility during the tests.

VIX. References

[1] A. C. Eckbreth, "Laser Diagnostics for Combustion Temperature and Species 2nd Edition", Combustion Science & Technology Book Series, Vol. 3, Taylor & Francis , New York, 2002

[2] S. O'Byrne, " Hypersonic Laminar Boundary Layers and Near-Wake Flows", *Ph.D. Thesis*, The Australian National University, 2001

[3] J.L. Palmer, B. K. McMillin, R. K. Henson, "Planar Laser-Induced Fluorescence Imaging of Velocity and Temperature in Shock Tunnel Free Jet Flow", *AIAA 92-0762, 30th Aerospace Sciences Meeting and Exhibit*, Reno, NV, 1992

[4] B.K. McMillin, J. L. Palmer, R. K. Henson, "Temporally Resolved, Two-Line Fluorescence Imaging of NO Temperature in a Transverse Jet in a Supersonic Cross Flow", *Applied Optics*, Vol. 32, No. 36, 1993

[5] F. Gray Kidd III, V. Narayanaswamy, P. M. Danehy, J. A. Inman, B. F. Bathel, K. F. Campbell, N. E. Hass, D. P. Capriotti, T. g. Drozda, " Characterization of the NASA Langley Arc Heated Scramjet Test Facility Using NO PLIF", *AIAA 2014-2652, 30th AIAA Aerodynamic Measurements Technology and Ground Testing Conference*, Atlanta, GA, 2014

[6] R. J. Hartfield, J. D. Abbitt, J. C. McDaniel. "Injectant mole-fraction imaging in compressible mixing flows using planar laser-induced iodine fluorescence", *Optics letters*, Vol. 14, No. 16, 1989, pp. 850-852

[7] J. M. Donohue, J. C. McDaniel, "Computer-controlled multiparameter flowfield measurements using planar laser-induced iodine fluorescence", *AIAA Journal*, Vol. 34, No. 8, 1996, pp. 1604-1611

[8] H. Takahashi, S. Ikegami, H. Oso, G. Masuya, M. Hirota, "Quantitative Imaging of Injectant Mole Fraction and Density in a Supersonic Mixing", *AIAA Journal*, Vol. 46, No. 11, 2008, pp. 2935-2943.

[9] C. C. Rasmussen, S. K. Dhanka, J. F. Driscoll, "Visualization o Flameholding Mechanism in a Supersonic Combustor Using PLIF", *Proceeding of the Combustion Institute*, Vol. 31, 2007, pp. 2505-2512

[10] J. M. Donbar, M. R. Gruber, T. A. Jackson, C. D. Carter, T. Mathur, "OH Planar Laser-Induced Fluorescence in a Hydrocarbon-Fueled Scramjet Combustor", *Proceeding of the Combustion Institute*, Vol. 28, 2000, pp. 679-687

[11] M. J. Gaston, A. F. P. Houwing, N. R. Mudford, P. M. Danehy, J. S. Fox, "Fluorescence imaging of mixing flowfields and comparisons with computational fluid dynamic simulations", *Shock Waves*, Vol. 12, No. 2, 2002, pp. 99-110

[12] M. R. Gruber, J. M. Donbar, C. D. Carter, K. Y. Hsu, "Mixing and Combustion Studies Using Cavity-Based Flameholder in a Supersonic Flow", *Journal of Propulsion and Power*, Vol. 20, No. 5, 2004, pp. 769-783

[13] F. W. Barnes, Q. Tu, C. Segal, "Mixing and Mass Exchange for Cavities in Supersonic Flow", *AIAA 2014-2951, 19th AIAA International Space Planes and Hypersonic Systems and Technology Conference*, Atlanta, GA, 2014

[14] A. Thakur, C. Segal, "Concentration Distribution in Supersonic Flow Recirculation Region", *Journal of Propulsion and Power*, Vol. 24, No. 1, 2008

[15] T. Rossmann, M. G. Mungal, R. K. Hanson, "Nitric-oxide planar laser-induced fluorescence applied to low-pressure hypersonic flow fields for the imaging of mixture fraction", *Applied Optics*, Vol. 42, No. 33, 2003, pp. 6682-6695

[16] T. Rossmann, M. G. Mungal, R. K. Hanson, "Mixing efficiency measurements using a modified cold chemistry technique", *Experiments in Fluids*, Vol. 37, No. 4, 2004, pp. 566-576

[17] R. D. Rockwell, C. P. Goyne, W. Haw, R.H. Krauss, J. C. McDaniel, C.J. Trefny, "Experimental Study of Test-Medium Vitiation Effect on Dual-Mode Scramjet Performance and Power", *Journal of Propulsion and Power*, Vol. 27, No. 5, 2011, pp. 1135-1142

[18] R.H. Krauss, J. C. McDaniel, J. E. Scott, R. B. Whitehurst, C. Segal, G. T. Mahoney, J. M. Childers, "Unique, Clean-Air, Continuous Flow, High-Stagnation-Temperature Facility for Supersonic Combustion Research", *AIAA 1988-3059*, 1988

[19] R. H. Krauss, J. C. McDaniel, "A Clean Air Continuous Flow Propulsion Facility", *AIAA 1992-3912*, 1992

[20] R. D. Rockwell, C. P. Goyne, B. Rice, H. Chelliah, J. C. McDaniel, J. Edwards, A. D. Cutler, P. M. Danehy, "Development of a Premixed Combustion Capability for Scramjet Combustion Experiment", *AIAA 2015-xxxx, AIAA Science and Technology Forum and Exposition*, Kissimmee, FL, 2015

[21] S. Emami, C. A. Trexler, A. H. Auslender, J. P. Weidner, "Experimental Investigation of Inlet-Combustor Isolators for a Dual-Mode Scramjet at Mach Number of 4", *NASA Technical Paper 3502*, 1995

[22] C. P. Goyne, C. G. Rodriguez, R. H. Krauss, J. C. McDaniel, C. R. McClinton, "Experimental and Numerical Study of a Dual-Mode Scramjet Combustor", *Journal of Propulsion and Power*, Vol. 22, No 3, 2006, pp. 481-189

[23] M. R. Gruber, J. M. Donbar, C. D. Carter, k. Y. Hsu, "Mixing and Combustion Studies Using Cavity-Based Flameholder in Supersonic Flow", *Journal of Propulsion and Power*, Vol. 20, No. 5, 2004

[24] A. D. Cutler, G. Magnotti, L. M. L. Cantu, E. C. A. Gallo, P. M. Danehy, R. D. Rockwell, C. P. Goyne, "Dual-Pump CARS Measurements in a Dual-Mode Scramjet", *Journal of Propulsion and Power*, Vol. 30, No. 3, 2014, pp. 539-549

[25] E. C. A. Gallo, L. M. L. Cantu, A. D. Cutler, M. J. Rahimi, H. K. Chelliah, "WIDECARS Measurements of Major Species Concentration and Temperature in an Air-Ethylene Flame", *AIAA 2014-2525, 30th AIAA Aerodynamic Measurement Technology and Ground Testing Conference*, Atlanta, GA, 2014

[26] J. S. Fox, A. F. P. Houwing, P. M. Danehy, M. J. Gaston, N. R. Mudford, S. L. Gai, "Mole-Fraction-Sensitive Imaging of Hypermixing Shear Layers", *Journal of Propulsion and Power*, Vol. 17, No. 2, 2001, pp. 284-292

[27] C. T. Johansen, C. D. McRae, P. M. Danehy, E. C. A. Gallo, L. M. L. Cantu, G. Magnotti, A. D. Cutler, "OH PLIF Visualization of the UVa Supersonic Combustion Experiment: Configuration A", *Journal of Visualization*, Vol. 17, No. 2, 2014, pp. 131-141

[28] J. R. Engleman, P. E. Rouse, "The β and γ Bands of Nitric Oxide Observed During the Flash Photolysis of Nitrosyl Chloride", *Journal of Molecular Spectroscopy*, No. 37, 1971, pp. 240 – 251

[29] P.C. Palma, "Laser Induced Fluorescence Imaging in Free-Piston Shock Tunnels", *Ph.D. Thesis*, The Australian National University, 1998

[30] J. Danielak, U. Domin,R. Kepa, M. Rytel, Zachwieja, "Reinvestiation of the Emission γ Band System ($A_2\Sigma^+$ - $X^2\Pi$) of the NO Molecule", *Journal of Molecular Spectroscopy*, No. 181, 1997 pp. 394-402

[31] M. D. DiRosa, "High-Resolution Line Shape Spectroscopy of Transitions in the Gamma Bands of Nitric Oxide", *Ph.D. Thesis*, Stanford University, 1996

[32] A. O. Vyrodov, J. Heinze, U. E. Meier, "Collisional Broadening of Spectral Lines in the A-X (0-0) System of NO by N_2, Ar, and He at Elevated Pressures Measured by Laser-Induced Fluorescence", *Journal of Quantitative Spectroscopy and Radiative Transfer*, Vol. 53, No. 3, 1995, pp. 277-287

[33] T. B. Settersten, B. D. Patterson, C. D. Carter, "Collisional Quenching of NO $A^2\Sigma^+$ (v'=0) Between 125 and 294 K", *The Journal of Chemical Physics*, Vol. 130, 2009

[34] P.H. Paul, J. A. Gray, J. L. Durant Jr., J. W. Thoman Jr., "Collisional Quenching Corrections for Laser-Induced Fluorescence Measurements of NO $A^2\Sigma^+$", *AIAA Journal*, Vol. 32, No.8, 1994, pp. 1670 – 1675

[35] C. D. McRae, C. T. Johansen, P. M. Danehy, E. C. A. Gallo, L. M. L. Cantu, G. Magnotti, A. D. Cutler, R. D. Rockwell, C. P. Goyne, J. C. McDaniel, "OH PLIF Visualization of the UVa Supersonic Combustion Experiment: Configuration C", *AIAA 2013-0034, 51st AIAA Aerospace Meeting*, Grapeville, TX, 2013

[36] J. A. Inman, P. M. Danehy, B. F. Bathel, D. W. Aldefer, R. J. Nowak, "Laser-Induced Fluorescence Velocity Measurements in Supersonic Underexpanded Impinging Jets", *AIAA 2010-1438, 48th AIAA Aerospace Sciences Meeting, Fluid Dynamics TC*, Orlando, FL, 2010

[37] W. S. Rasband, ImageJ, US National Institute of Health, Bethesda, MD, USA, http://rsb.info.nih.gov/ij, 1997-2009

[38] C. Ó. Sánchez Sorzano, P. Thévenaz, M. Unser, "Elastic Registration of Biological Images Using Vector-Spline Regularization ," *IEEE Transactions on Biomedical Engineering*, vol. 52, no. 4, pp. 652-663, April 2005